Received April 2001
Accepted January 2002

Numerical study of fluid flow through double bell-shaped constrictions in a tube

T.S. Lee
National University of Singapore, Singapore

Keywords *Flow, Tubing*

Abstract *The effects of steady fluid flow through double bell-shaped constrictions in tubes were investigated numerically for the Reynolds number range of 5 to 400. The double constrictions studied were for similar first and second constrictions of 1/3, 1/2 and 2/3. A dimensionless constriction spacing of 1.0 was considered. Study showed that the major part of the mean dimensionless pressure drop in the constricted tube occurs predominantly across the first constriction when flow moves towards the valley region formed by the two constrictions. Minimum pressures along the constricted tubes occurs downstream of each constrictions. When the constriction magnitudes increased, the pressure drop across the same length of the tube increases exponentially. The effect of increasing the Reynolds number for all the constriction values considered here is to increase the spreading of the recirculation region between the valley region of the constrictions. The recirculation region formed between the two constrictions has a deminishing effect on the generation of wall vorticity near the second constriction. The effects are more pronounce when the recirculatory flow from the first constriction has spread over the second constriction. In general, a peak wall vorticity is found slightly upstream of each of the constrictions. When the Reynolds number is increased, the peak wall vorticity increases and its location moved upstream. It is noted for the cases considered here that the peak wall vorticity generated by the first constriction is always greater than the peak wall vorticity generated by the second constriction.*

Nomenclature

a_0 = radius of the constant cross section of the tube
c_1 = dimensionless up-stream (first) constriction, $c_1 = (d - d_1)/d$
c_2 = dimensionless down-stream (second) constriction, $c_2 = (d - d_2)/d$
d = diameter of constant cross section of the tube
d_1 = diameter of the tube at the first constriction
d_2 = diameter of the tube at the second constriction
L = length of the tube
l_1 = location of up-stream (first) constriction
l_2 = location of down-stream (second) constriction
P_0 = axial static pressure at inlet
$P_{\min}$ = minimum pressure
P^* = dimensionless pressure, $P^* = (P - P_0)/(\rho v_0^2)$
ΔP = mean dimensionless pressure difference between two point,
(r, z) = co-ordinates variables in the original cylindrical co-ordinate system
Re = Reynolds number, $\mathrm{Re} = v_0 a_0/\nu$
S = dimensionless spacing between constrictions, $S = (l_2 - l_1)/d$
t = time
u = radial velocity component
v = axial velocity component
v_0 = centreline velocity at inlet plane

International Journal of Numerical Methods for Heat & Fluid Flow, Vol. 12 No. 3, 2002, pp. 258-289.

DOI 10.1108/09615530210422947

Greek symbols

ψ = stream function
ζ = vorticity
$(\zeta_w)_{max}$ = Peak wall vorticity
ρ = density
ν = kinematic viscosity
ω = relaxation factor in SOR
(η, ϵ) = co-ordinates variables in the transformed co-ordinate system

Subscripts

w = wall
c = centreline

Introduction

The flow field in the neighbourhood of various shapes of constriction in tubes are of great interest to fluid dynamicists and engineers. This type of tube configuration is used in heat exchangers in order to enhance its heat transfer performances. The wavy configuration of tubes has also been of great interest to biofluid dynamicists because of its relationship to localised stenoses; blood and urinary flow; and for the optimal design of artificial organs. Viscous fluid flow past wavy boundaries has also been of great interest to engineers and researchers because of the importance it plays in phenomena such as: the generation of wind waves on water; the stability of a liquid film in contact with a gas stream; the transpiration cooling of re-entry vehicles and rocket boosters; film vaporization in combustion; fluid flow in pipes with fittings.

An early numerical work on constriction in tube was first done by Lee and Fung (1970). A bell-shaped constriction specified by a Gaussian normal distribution curve was used to simulate flow in locally constricted tubes. Reynolds number in the range of 0 to 25 was considered. Numerical instability in the solution procedure prevented the investigation from extending to higher Reynolds Number. Similar numerical studies were carried out by Oberkampt and Goh (1974). An outflow type of boundary condition was used by Lee & Fung, whilst Oberkampt & Goh used an infinity condition. Constrictions with other type of shapes such as a sinusoidal function was used by Despande *et al.* (1976) to model the steady laminar flow through vascular stenoses. The separating flow through a severely constricted symmetric tube was studied analytically. The main separation was shown to take place on the upstream constriction surface. Sobey (1980) studied numerically the flow through furrowed channels and investigated the Reynolds number effects on the separated flow. Patankar *et al.* (1977), Sparrow and Prata (1983) and Prata and Sparrow (1984) obtained numerical solutions for a periodic fully developed sinusoidal flow regime in an annulus of varying cross section of a double-pipe in a heat exchanger. On the basis of the computed heat transfer coefficients and pressure drops, the periodic sinusoidal undulating annulus appears to be an attractive enhancement configuration relative to the annulus of axially unchanging cross section. Other related studies of constricted flow includes a study of laminar steady flow in sinusiodal channels by Tsangaris and Leiter (1984) using a perturbation technique. Dreumel and Kuiken (1989) did a

numerical and experimental study on flow past a double stenosis tube. Sharp edges were used in the experimental set-up for the coronary stenosis (62 per cent) and flow was analyzed for Re in the range of 50–400. For low Re, the total effect of 2 stenosis was noted to be equals to twice that of a single one for the pressure distribution.

More recently in the 1990s, Johnston and Kilpatrick (1991) did a similar analysis of flow through an irregularly shaped arterial stenosis with area reduction varying from 48 per cent to 87 per cent. Cheng *et al.* (1992) revised the problem of flow through stenosis by considering a steady flow under finer mesh and more realistic Reynold number conditions. The effect of varying the degree of stenosis, structure length, Reynolds Number was studied. Najeme *et al.* (1992) did a numerical analysis of flow over stenoses with an asymptotic method for low as well as large Reynolds Number of 1000. The velocity profile was approximated with a polynomial of degree m. Tutty (1992) analyzed flow over a non-uniform channel as a model for a constricted blood vessel. Flow patterns were found for a range of Reynolds Number. The resulting waveform shows strong vortex and complex wall shear stress distribution. The imposed inflow is found to have an impact on the flow and stress distribution. Rosenfeld and Einav (1993) attempts analytically to verify the results of numerical analysis of flow over a constriction in a channel. Numerical simulation was done with a fractional time step method and the resulting flow yield a series of moving vortices. Factors which affects the validity of the solution, like mesh size, time-step refinement studies, boundary conditions etc. were looked examined. Cavalcanti and Carota (1995) theoretically investigated haemodynamics in the early stages of the artherosclerotic process. It aims to provide more information on the velocity flow field as induced by a mild stenosis (with area reduction of only 2 per cent). It was hope that, with more high resolution velocimetry coming up in the future, detection of stenosis-formation can be done even before they become clinically significant, by virtue of the altered flow field. Huang *et al.* (1995) investigated the cause for development of a therosclerosclerosis lesion by doing a numerical study on flow in a rigid tube with an occlusion. The results show a good correlation between regions of recirculation and the location of lension. Rosenfeld and Einav (1995) further studied the effect of constriction size on flow in a channel. It was found out that even for small constriction size, large number of vortices was created downstream of the constriction and the strength and number increases with area occlusion. However, the maximal size and the propagation size of the vortices were noted by them to be independent of the constriction size. It was hoped that the findings could help in non-invasive detection of severity and formation of stenoses and the potential damage to blood elements due to vortices. Damodaran *et al.* (1996) did a study of steady laminar flow over multiple constrictions for Reynolds Number in the range of 50–250 with 75 per cent area reduction for constrictions. Bluestein, Niu, Schoephoerster & Dewanjee (1997) studied fluid flow through a model

stenosis using both numerical and experimental methods with Reynolds Number ranging from 300 to 3600. A progressively dense mesh grid size was adopted near the wall and inlet region to capture the plug flow velocity profile at the inlet. Their result showed that the flow is turbulent at the throat, leading to an axi-symmetical and slowly circulating flow distal to the throat. As the Reynolds Number increased, the recirculation region became more disturbed. Siouffi *et al.* (1998) also did an experiment on flow through a stenosis. The flow region distal to the stenosis is analyzed with a pulsed Doppler ultrasonic velocimeter. It was noted, besides the usual flow parameters, the velocity field also depends on the flow waveform distal to the constriction. Reese and Thompson (1998) utilized the laminar momentum integral equation to simulate the shear stress in an arterial stenosis. Fluid flow with up to Reynolds number of 1000 were simulated and analyzed. The reductions of the constricted areas were between 44 per cent and 75 per cent. The final results obtained compared well with known results from Poiseuille flow in a pipe. Selvarajan *et al.* (1998) applied a perturbation method in analyzing the flow through wavy-walled channels. This numerical study looked into the aspects of the development of asymmetry at low Reynolds numbers. Computations at $\mathrm{Re} = 0.6$ revealed that the initial development of asymmetry. Further values of $\mathrm{Re} = 0.06$, 0.006, and 0.001 were used and it was found that the flow field gains symmetry as Re reached 0.001. The Reynolds number and amplitude parameter were noted to affect the skin friction on the wavy wall. These two parameters were used to indicate the location of separation and reattachment of the fluid field. Cieslicki and Lasowska (1999) studied the problem of a steady flow in a tube with circumferential wall cavity with Reynolds number of 0, 50 and 200. Dash *et al.* (1999) studied the mechanics of blood flow in a catherized curved artery with stenosis through a mathematical analysis. The properties of the blood flow field were studied in the presence of the curvature of the blood vessel, stenosis and catheter. The Reynolds number considered ranges from 25 to 100. The combined effect were studied and it concluded that the presence of stenosis was more dominant in affecting the properties of the flow field. Deplano and Siouffi (1999) carried out investigation on the effect of flows through stenosis both experimentally and numerically. It was found that high shear stress was produced at the throat.

For work in the 2000s, Hron *et al.* (2000) had carried out numerical work on flow of shear-thinning fluids. A solver developed by Turek had been modified for the purpose of this study. Shear-thinning fluids are fluids where the viscosity decreases for the increasing shear rate. This phenomenon is applicable to blood rheology. Reynolds number ranging from 1 to 1000 and an aspect ratio ($A = 1.0 - c$) of 0 and 0.5 were chosen for the studies. Stroud *et al.* (2000) studied on the various reasons that contributed to the plaque rupture. The author believed that percentage reduction of the artery diameter was not the only major cause of major heart abnormality, other factors such as the stenosis morphology, surface irregularities, and the shape of the pulsatile

waveform were also possible factors. This paper provided information on the flow field when the stenosis was not axisymmetry. It was found that slight changes to the curvature and surface irregularities made substantial impact on the flow field.

In the above studies, few consider the influence of multiple constrictions in the flow filed of a tube. In this present work, the detailed flow behaviour in a double bell-shaped constricted tubes are studied. In order to provide accuracy numerical solutions and better resolutions for flow field near the constrictions, the physical domain of the double bell-shaped constricted tube is first transformed into a rectangular solution domain using a generalized mapping function. A progressively dense mesh was adopted near the wall region to carefully track the flow information near the wall region as well as to better capture the shear flow velocity profile at the wall. The dynamics of the flow describing separation, reattachment, and the formation of recirculation eddy were studied through the developing streamline, velocity vectors, vorticity and pressure fields. Numerical results are obtained for the Reynolds number in the range of 5 to 400 with constriction ratio of 1/3, 1/2 and 2/3 for a pair closely spaced ($S = 1.0$) constrictions. The preliminary findings of the present study on single constriction flow were also compared with available experimental and numerical work of other investigators.

Problem formulation

The geometry of the constricted tube is shown in Figure 1(a). The constrictions are modelled by 2 Guassian normal distribution curve, given by

$$\begin{aligned} r &= 1 - c_1 \exp[-k(z - l_1)^2] \quad (l_1 - l_k) < z < (l_1 + l_k) \\ r &= 1 - c_2 \exp[-k(z - l_2)^2] \quad (l_2 - l_k) < z < (l_2 + l_k) \\ r &= 1 \qquad\qquad\qquad\qquad\quad \text{elsewhere} \end{aligned} \tag{1}$$

where $c_1 = (d - d_1)/d$ and $c_2 = (d - d_2)/d$ are the constriction ratios; l_1, l_2 are the locations for the first and second constrictions respectively with respect to the inlet location; l_k defined the domain of the constrictions concerned. For the present studies with $k = 4.0, l_k = 1.0$ provides a smooth transition between the solution domains. The constriction spacing is given by $S = l_2 - l_1$.

Taking the cylinder radius (a_0) and the centreline velocity at inlet (v_0) as the characteristic length and velocity respectively, the following non-dimensional variables are defined:

$$r^* = \frac{r}{a_0}, v^* = \frac{v}{v_0}, \psi^* = \frac{\psi}{v_0 a_o^2}, t^* = \frac{tv_0}{a_0}, u^* = \frac{u}{v_0}, z^* = \frac{z}{a_0}, \zeta^* = \frac{\zeta a_0}{v_0}. \tag{2}$$

The unsteady governing equations are used to solve for the steady state flow fields considered in this study. Constant fluid properties are assumed. The flow is considered axis-symmetric and laminar. The dimensionless governing

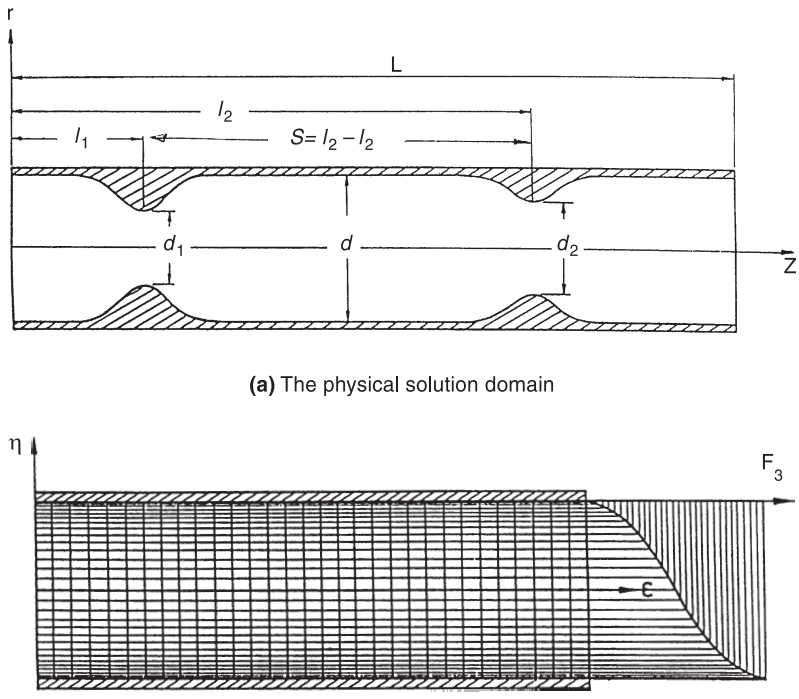

(a) The physical solution domain

(b) The transformed computational solution domain

Figure 1.
Model of double bell-shaped constrictions in tubes

equations in the form of stream function-vorticity relations expressed in cylindrical co-ordinates (r, θ, z) for the axis-symmetrical flow in the constricted tubes [omitting the superscript * for brevity] are:

$$\frac{\partial \zeta}{\partial t} + \frac{\partial u\zeta}{\partial r} + \frac{\partial v\zeta}{\partial z} = \frac{1}{\mathrm{Re}}\left[\frac{\partial^2 \zeta}{\partial r^2} + \frac{\partial^2 \zeta}{\partial z^2} + \frac{1}{r}\frac{\partial \zeta}{\partial r} - \frac{\zeta}{r^2}\right] \tag{3}$$

$$\zeta = \frac{1}{r}\left[-\frac{1}{r}\frac{\partial \psi}{\partial r} + \frac{\partial^2 \psi}{\partial z^2} + \frac{\partial^2 \psi}{\partial r^2}\right] \tag{4}$$

$$u^* = \frac{1}{r}\frac{\partial \psi}{\partial z} \quad \text{and} \quad v^* = -\frac{1}{r}\frac{\partial \psi}{\partial r} \tag{5}$$

The Reynolds number is defined as $\mathrm{Re} = v_0 a_0/\nu$. Axis-symmetrical flow conditions are assumed. At the inlet, the velocity profile is assumed to be Poiseuille, given by:

$$\frac{v}{v_0} = 1 - \left(\frac{r}{a_0}\right)^2 \quad \text{and} \quad u = 0 \tag{6}$$

The stream function and vorticity distribution at the inlet are derived from the integration of the above velocity conditions. Along the solid tube walls, non-slip conditions are assumed, i.e. $v = u = 0$.

The governing equation for the pressure solution is given by the Poisson equation,

$$\frac{\partial^2 P}{\partial z^2} + \frac{\partial^2 P}{\partial r^2} + \frac{1}{r}\frac{\partial^2 \psi}{\partial z^2} = \frac{2}{r^2}\left[\frac{\partial^2 \psi}{\partial z^2}\left(\frac{\partial^2 \psi}{\partial r^2} - \frac{1}{r}\frac{\partial \psi}{\partial r}\right) - \frac{1}{r^2}\left(\frac{\partial \psi}{\partial z}\right)^2 + \frac{\partial^2 \psi}{\partial r \partial z}\left(\frac{1}{r}\frac{\partial \psi}{\partial z} - \frac{\partial^2 \psi}{\partial r \partial z}\right)\right] \tag{7}$$

where the non-dimensional pressure is $P^* = P - P_0/\rho v_0^2$, where P_0 is the static pressure at the inlet.

Along the tube wall, in the r-direction [omitting the superscript * for brevity],

$$\frac{\partial P}{\partial r} = \frac{1}{\mathrm{Re}}\frac{\partial \zeta}{\partial z} \tag{8}$$

In the z-direction,

$$\frac{\partial P}{\partial z} = -\frac{1}{\mathrm{Re}}\left(\frac{\partial \zeta}{\partial r} + \frac{\zeta}{r}\right) \tag{9}$$

Numerical solution

The cylindrical co-ordinate system (r, z) as shown in Figure 1(a) is not suitable for the accurate evaluation of boundary conditions on the curved surface of the constricted physical solution domain. Hence, a generalised simple co-ordinate transformation technique is used to transform the complex curvaceous tube profile to a plain rectangular solution domain as shown in Figure 1(b). The new co-ordinate system is

$$\varepsilon = z; \eta = \frac{r}{f_1(z)} \tag{10}$$

where $f_1(z)$ is a function used to describe the curved boundaries. Expressing the partial derivatives in the rectangular transformed domain, the governing transport equations become:

$$\begin{aligned}
&\frac{\partial \zeta}{\partial t} + \frac{\partial (u\zeta)}{\partial \eta}\frac{\partial \eta}{\partial r} + \frac{\partial (v\zeta)}{\partial \varepsilon}\frac{\partial \varepsilon}{\partial r} + \frac{\partial (v\zeta)}{\partial \eta}\frac{\partial \eta}{\partial z} \\
&\quad = \frac{1}{\mathrm{Re}}\left[\frac{\partial^2 \zeta}{\partial \eta^2}\left\{\left(\frac{\partial \eta}{\partial r}\right)^2 + \left(\frac{\partial \eta}{\partial z}\right)^2\right\} + \frac{\partial^2 \zeta}{\partial \eta^2}\left(\frac{\partial \varepsilon}{\partial z}\right)^2\right. \\
&\qquad \left. + \frac{\partial^2 \zeta}{\partial \eta \partial \varepsilon}\left(2\frac{\partial \eta}{\partial z}\frac{\partial \varepsilon}{\partial z}\right) + \frac{\partial \zeta}{\partial \eta}\left\{\frac{\partial^2 \eta}{\partial z^2} + \frac{1}{r}\frac{\partial \eta}{\partial r}\right\} + \frac{\partial \varepsilon}{\partial z}\left(\frac{\partial^2 \varepsilon}{\partial z^2}\right)^2 - \frac{\zeta}{r^2}\right]
\end{aligned} \tag{11}$$

$$\zeta = \frac{1}{r}\left[\frac{\partial^2\psi}{\partial\eta^2}\left\{\left(\frac{\partial\eta}{\partial r}\right)^2+\left(\frac{\partial\eta}{\partial z}\right)^2\right\}+\frac{\partial^2\psi}{\partial\varepsilon^2}\left(\frac{\partial\varepsilon}{\partial z}\right)^2\right] + \frac{\partial^2\psi}{\partial\varepsilon\partial\eta}\left(2\frac{\partial\eta}{\partial z}\frac{\partial\varepsilon}{\partial z}\right)+\frac{\partial\psi}{\partial\varepsilon}\left(\frac{\partial^2\varepsilon}{\partial z^2}\right)+\frac{\partial\psi}{\partial\eta}\left(\frac{\partial^2\eta}{\partial z^2}-\frac{1}{r}\frac{\partial\eta}{\partial r}\right)\Bigg] \tag{12}$$

$$\frac{\partial^2 P}{\partial\eta^2}\left(\frac{\mathrm{d}\eta}{\mathrm{d}z}\right)^2+\frac{\partial^2 P}{\partial\varepsilon^2}+2\frac{\partial^2 P}{\partial\eta\partial\varepsilon}\frac{\mathrm{d}\eta}{\mathrm{d}z}+\frac{\partial P}{\partial\eta}\frac{\mathrm{d}^2\eta}{\mathrm{d}z^2}+\frac{\partial^2 P}{\partial\eta^2}\left(\frac{\mathrm{d}\eta}{\mathrm{d}r}\right)^2+\frac{1}{r}\frac{\partial P}{\partial\eta}\frac{\mathrm{d}\eta}{\mathrm{d}r}$$

$$= \frac{2}{r^2}\left[\begin{array}{l}\left(\frac{\partial^2\psi}{\partial\eta^2}\left(\frac{\mathrm{d}\eta}{\mathrm{d}z}\right)^2+\frac{\partial^2\psi}{\partial\varepsilon^2}+2\frac{\partial^2\psi}{\partial\eta\partial\varepsilon}\frac{\mathrm{d}\eta}{\mathrm{d}z}+\frac{\partial\psi}{\partial\eta}\frac{\mathrm{d}^2\eta}{\mathrm{d}z^2}\right)\left(\frac{\partial^2\psi}{\partial\eta^2}\left(\frac{\mathrm{d}\eta}{\mathrm{d}r}\right)^2-\frac{1}{r}\frac{\partial\psi}{\partial\eta}\frac{\mathrm{d}\eta}{\mathrm{d}r}\right)\\ -\frac{1}{r^2}\left(\frac{\partial\psi}{\partial\eta}\frac{\mathrm{d}\eta}{\mathrm{d}z}+\frac{\partial\psi}{\partial\varepsilon}\right)^2+\left(\left(\frac{\partial^2\psi}{\partial\eta^2}\frac{\mathrm{d}\eta}{\mathrm{d}z}+\frac{\partial^2\psi}{\partial\eta\partial\varepsilon}\right)\frac{\mathrm{d}\eta}{\mathrm{d}r}+\frac{\partial\psi}{\partial\eta}\frac{\mathrm{d}^2\eta}{\mathrm{d}r\mathrm{d}z}\right)\\ \left(\frac{1}{r}\left(\frac{\partial\psi}{\partial\eta}\frac{\mathrm{d}\eta}{\mathrm{d}z}+\frac{\partial\psi}{\partial\varepsilon}\right)-\left(\frac{\partial^2\psi}{\partial\eta^2}\frac{\mathrm{d}\eta}{\mathrm{d}z}+\frac{\partial^2\psi}{\partial\eta\partial\varepsilon}\right)\frac{\mathrm{d}\eta}{\mathrm{d}r}+\frac{\partial\psi}{\partial\eta}\frac{\mathrm{d}^2\eta}{\mathrm{d}r\mathrm{d}z}\right)\end{array}\right] \tag{13}$$

where $z = \varepsilon$; $r = \eta f(\varepsilon)$ and $\mathrm{d}\varepsilon/\mathrm{d}r = 0$; $\mathrm{d}\varepsilon/\mathrm{d}z = 1$. The corresponding wall pressure equations (8) and (9) and vorticity at the wall boundary can be expressed as

$$\frac{\partial P}{\partial\eta}\frac{\mathrm{d}\eta}{\mathrm{d}r} = \frac{1}{\mathrm{Re}}\left(\frac{\partial\zeta}{\partial\eta}\frac{\mathrm{d}\eta}{\mathrm{d}z}+\frac{\partial\zeta}{\partial\varepsilon}\right) \tag{14a}$$

$$\frac{\partial P}{\partial\eta}\frac{\mathrm{d}\eta}{\mathrm{d}z}+\frac{\partial P}{\partial\varepsilon} = -\frac{1}{\mathrm{Re}}\left(\frac{\partial\zeta}{\partial\eta}\frac{\mathrm{d}\eta}{\mathrm{d}z}+\frac{\zeta}{r}\right) \tag{14b}$$

$$\zeta_{\mathrm{w}} = \frac{1}{r}\left[\frac{\partial^2\psi}{\partial\eta^2}\left\{\left(\frac{\partial\eta}{\partial r}\right)^2+\left(\frac{\partial\eta}{\partial z}\right)^2\right\}+\frac{\partial^2\psi}{\partial\varepsilon\partial\eta}\left(2\frac{\partial\eta}{\partial z}\frac{\partial\varepsilon}{\partial z}\right)+\frac{\partial\psi}{\partial\eta}\left(\frac{\partial^2\eta}{\partial z^2}-\frac{1}{r}\frac{\partial\eta}{\partial r}\right)\right]_{\mathrm{wall}} \tag{14c}$$

The inlet boundary conditions for the stream-function is given by

$$\psi(\eta) = \psi_{\mathrm{c}} + \int_{\eta=0}^{\eta} v(\eta)\mathrm{d}\eta \tag{15}$$

The centreline stream function $\psi_{\mathrm{c}} = 0.0$ at $\eta = 0$ (corresponding to $r = 0$). At the wall, the stream function ψ_{w} is given by (15) with $\eta = 1$ (corresponding to $r = 1$).

Velocities u and v at the wall are assumed zero.

The domain in the $\varepsilon - \eta$ co-ordinate system as defined by Equation (10) is a rectangular region. In order to obtain better resolution of the solution near the wall regions while preserving the second order accuracy of the finite difference scheme, the rectangular solution domain is overlaid with a non-uniform mesh with the grid generator as shown in Figure 1(b) and given by

$$F_3 = (2/\pi)\sin^{-1}[(\eta + 0.5)^{1/2}] \tag{16}$$

At the node points, the finite difference solution to Equation (11) and its boundary conditions are obtained through an Alternating Direction Implicit (ADI) procedure by Samarskii and Andrew (1963). The Successive Over Relaxation (SOR) method with a relaxation parameter $\omega = 1.1$ is used to solve the vorticity-stream function equation (12). The pressure field described by equation (13) with its associated boundary conditions are obtained directly from the streamline field. All spatial derivatives are approximated by second-order-accurate central differences. The convective terms in equation (11) are approximated by the second-order upwind differencing method. Three points backward and forward difference formulae are used for the derivatives at the boundaries. The vorticity boundary values are obtained by considering the Taylor series expansion of ψ into the solution region and taking into consideration the ψ and the velocity at the boundary. Mesh independence studies were made and the final optimum mesh size arrived at for all the solutions presented here is 61×451. *For the present investigations, the optimum mesh size is the minimum computational mesh points used where the most severe flow condition of* $\mathrm{Re} = 400$ *with constriction of 2/3 and* $s = 1.0$ *produce results that are consistent with the estimated experimental results obtained by other investigators*. The steady state solution of the equations (11) and (12) is said to have converged when a difference less than 0.001 per cent of a referenced ψ and ζ is detected for a consecutive 100 iterations. This has proved satisfactory. The streamfunction contours, the velocity fields, the vorticity contours and the pressure field are noted to be steady after the above criteria are satisfied. *Details of the above numerical methods are also described in Lee (1994, 1998).*

Results and discussions

Most the existing related analytical, numerical and experimental studies are for fluid flow through single constrictions. Very few considered the influence of the upstream constriction on the flow field near the downstream constriction. Thus, for the purpose of validations, the present model was initially analysed for single constriction by setting $\mathrm{S} = \infty$ or $c_2 = 0$. Figure 2 showed that for $c_2 \Rightarrow 0$ or by increasing the constriction spacing $S \Rightarrow \infty$, flow over a single constriction is obtained. This study is similar to that of Lee and Fung (1970) where numerical results were obtained for Reynolds number in the range of

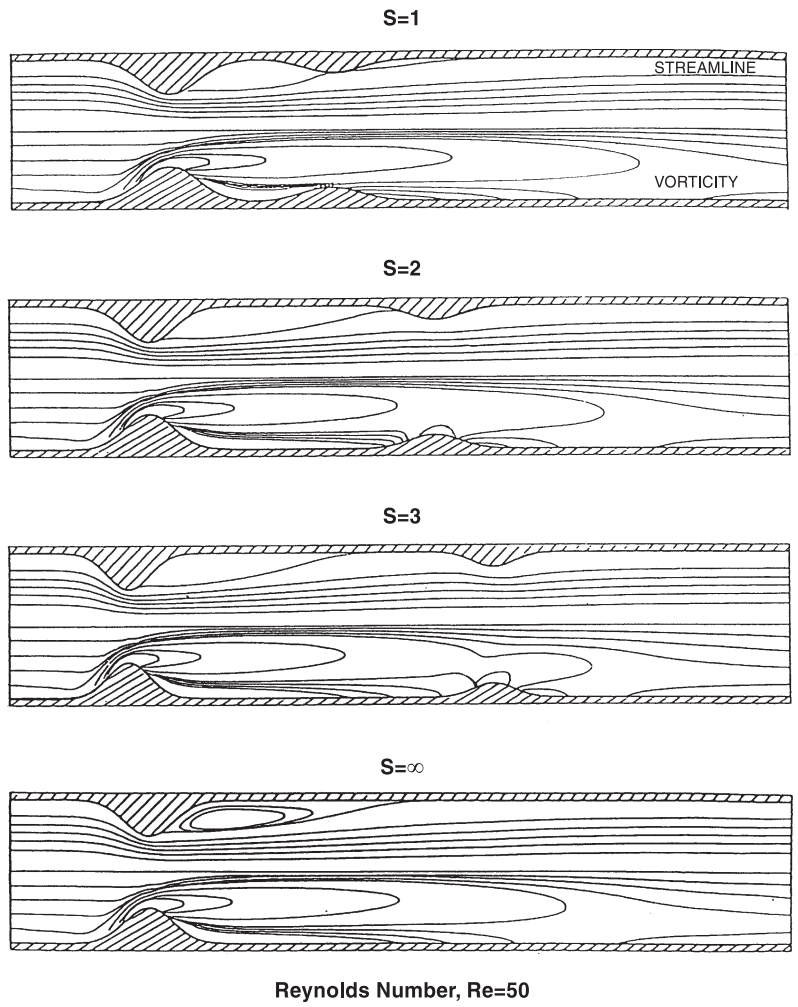

Figure 2.
Development of single constriction flow from double constrictions flow

0 to 25. Their streamlines, vorticity and velocity profiles show striking similarities with the present investigations in the available Reynolds number range of 5 to 25. At Re = 9.9, an eddy was observed near the downstream of the constriction by Lee and Fung. Similar eddy was also observed from the present study at Re = 10. For the present investigation with S = ∞ (Figure 3(b)), the peak wall vorticity value is 24.02 at Reynolds number of 5, and is increased to 57.31 when the Reynolds number is increased to 200. Lee and Fung obtained maximum wall vorticity of 28.5 and 36.5 at Reynolds numbers of 10 and 25, respectively. The corresponding values obtained in the present investigation are 24.62 and 29.84. Another similar study was performed by Deshpande *et al.*, 1976. Their

results were also presented on the same curve. The difference is believed to be due to the manner in which the outlet boundary condition was formulated. Lee and Fung assumed the outflow was Poiseuille and Deshpande, Giddens and Mabon assumed similar Poiseulle flow at $z \Rightarrow \infty$, whilst the present study assumed an unrestrictive flow at the outlet and allows the flow profile to develop on its own. *This is achieved through a series expansion of the flow field from the inner region towards the out flow region so that a steady and converged solution at the out flow boundary is obtained. Young and Tsai (1973) conducted a series of steady flow experiments for various hydrodynamic factors such as pressure drop, separation and turbulence on constriction flow. Comparisons of the present method of computations with the experimental work of Young & Tsai (1973) (Figure 3(a) and 3(c)) and Forrester and Young (1970) (Figure 3(a)) on single constriction flow showed very good agreement.*

Characteristics of (i) velocity vectors, (ii) streamline contours, (iii) pressure contours, (iv) centreline and wall pressure distribution, (v) vorticity contours, (vi) wall vorticity distribution and their associated recirculating flow region, maximum wall vorticity and pressure losses characteristics are investigated for constriction c_1, c_2 of (a) 1/3, (b) 1/2 and (c) 2/3 respectively for $\mathrm{Re} = 5$ (Figure 4), $\mathrm{Re} = 25$ (Figure 5) and $\mathrm{Re} = 50$ (Figure 6). For the Reynolds number of 5–400 considered here, a ring vortex might be developed downstream of a stenosis caused by flow separation. *For Reynolds number greater than 400, numerical experiments showed signs that the flow will become unstable and three dimensional effects will be developed, especially when the constrictions are severe.*

At a $\mathrm{Re} \ll 5$ (Figure 4), flow around each constriction of the double constrictions tube behaves similar to an independent single constriction tube without much interference of the flow from each other. Hence the vorticity contours are also similar near each of the constriction. No recirculation region appears in the constricted tube. As the Re increases, a recirculation eddy generally appears at downstream of each of the constrictions. As Re is further increased (Figure 5), recirculation regions appears for the constrictions considered here. The vorticity fields are substantially altered and the closed contours of the vorticity distribution are seen advected from each constrictions to the downstream. The recirculatory eddy from the upstream constriction is also spreaded downstream and affect the flow passing through the downstream constriction. A recirculation zone is than formed which fills part of the valley region between the two constrictions. Once the recirculation flow field between the constrictions is established, there is a separation streamline that divides the flow into two parts: the recirculating flow field between the two constrictions and the main flow field near the centre of the tube with relatively straight and parallel streamlines.

Characteristics of the flow through constrictions can also be described by the velocity vector in the tube. The velocity vectors in Figures 4(i)–6(i) show that as the fluid approaches the converging portion of the constriction, the

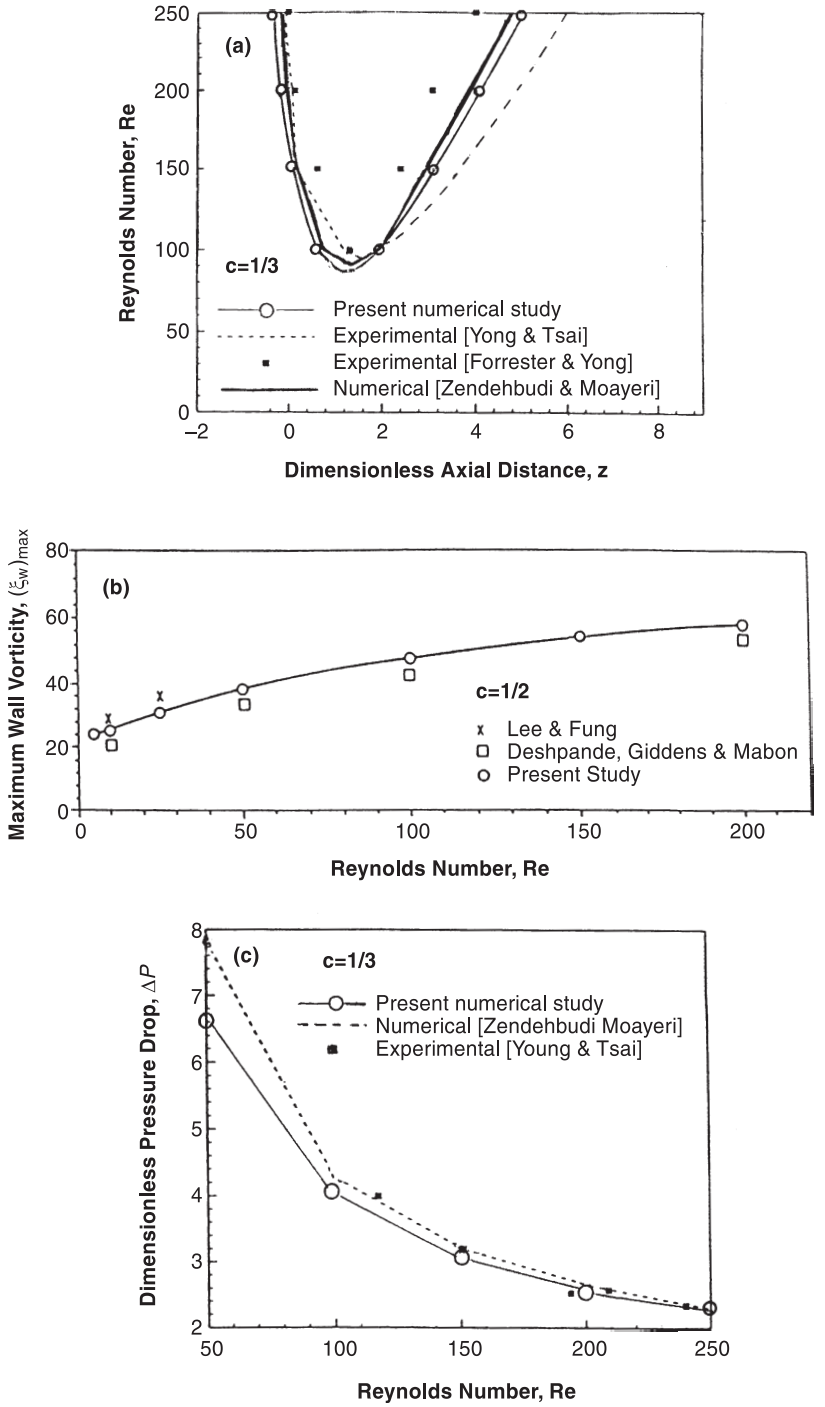

Figure 3.
Comparisons with available results of others

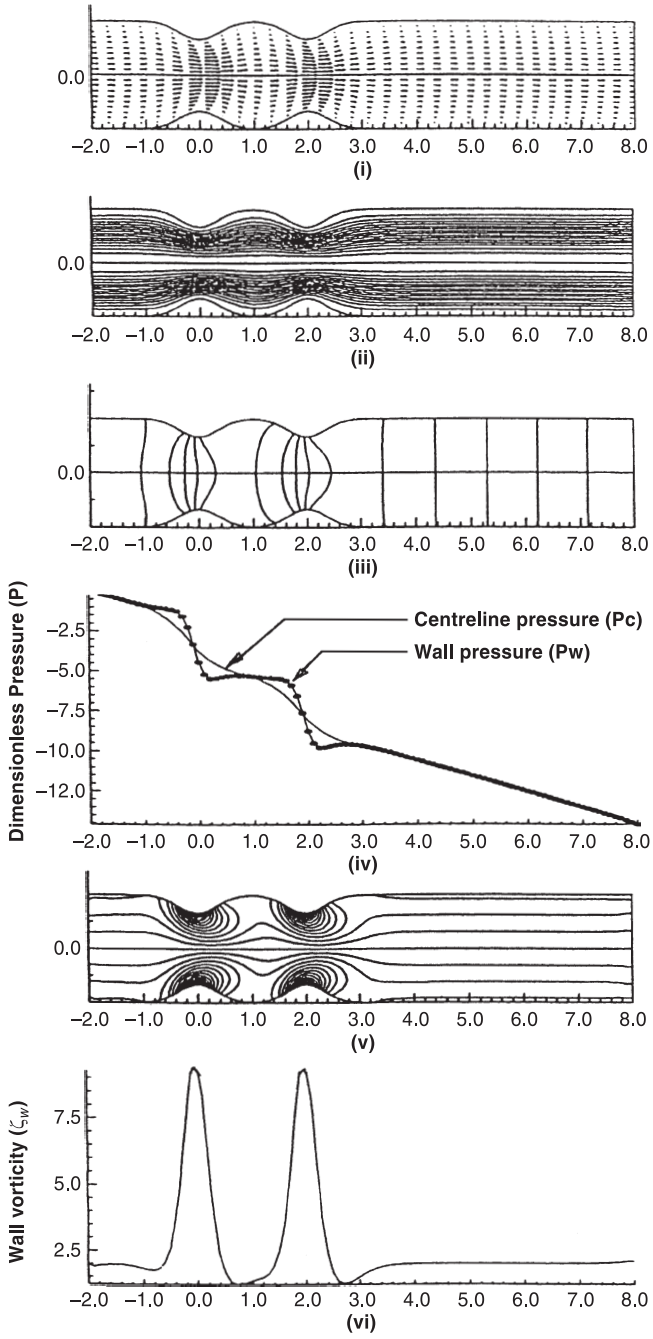

Figure 4.
(a) Re = 5; $c_1 = c_2 = 1/3$ (i) Velocity vectors; (ii) Streamlines; (iii) Pressure contours; (iv) Centreline (Pc) and Wall (Pw) pressures; (v) Vorticity contours; (vi) Wall vorticity (ζ_w) (b) Re = 5; $c_1 = c_2 = 1/2$ (i) Velocity vectors; (ii) Streamlines; (iii) Pressure contours; (iv) Centreline (Pc) and Wall (Pw) pressures; (v) Vorticity contours; (vi) Wall vorticity (ζ_w) (c) Re = 5; $c_1 = c_2 = 2/3$ (i) Velocity vectors; (ii) Streamlines; (iii) Pressure contours; (iv) Centreline (Pc) and Wall (Pw) pressures; (v) Vorticity contours; (vi) Wall vorticity (ζ_w)

(*Continued*)

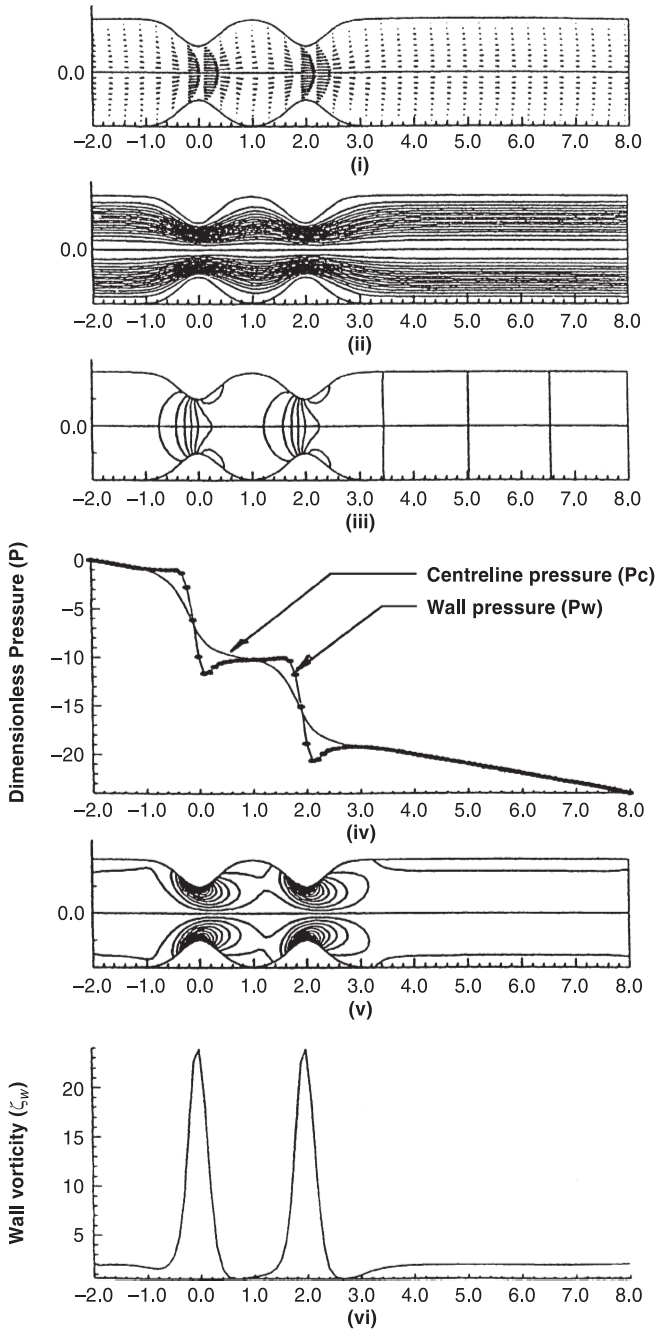

(*Continued*)

Figure 4.

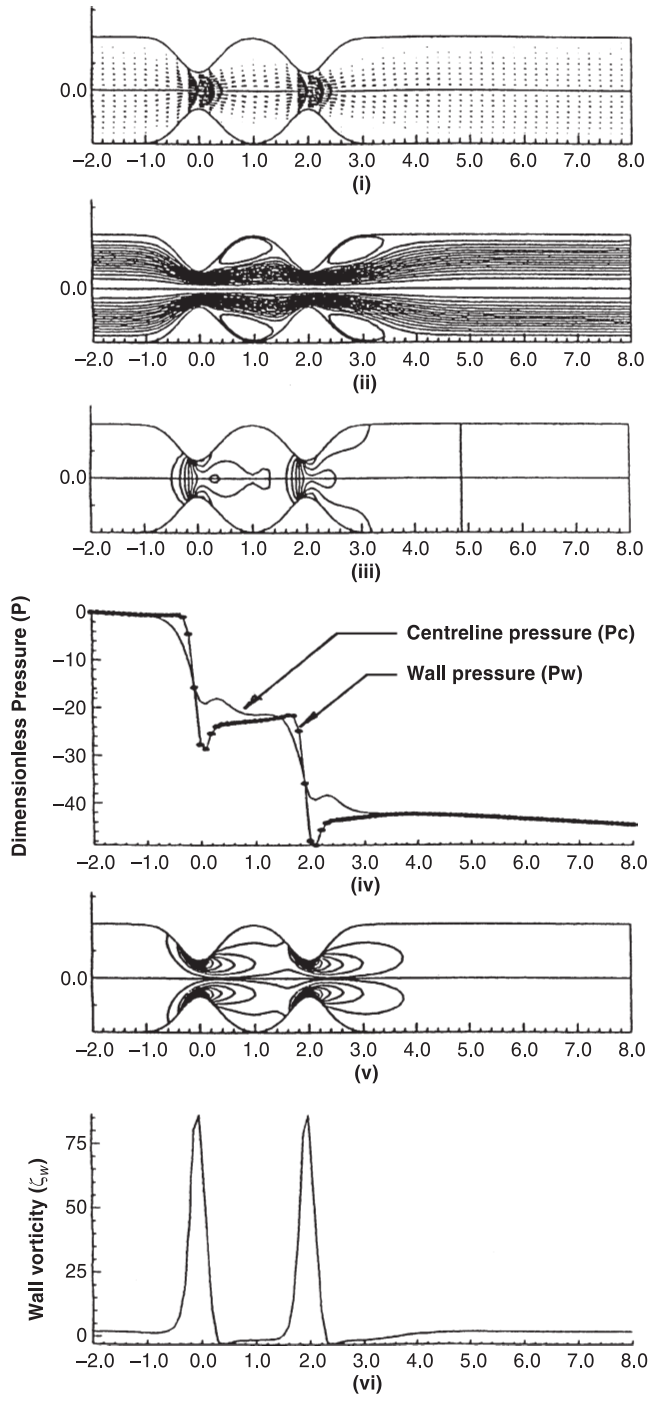
0.0
−2.0 −1.0 0.0 1.0 2.0 3.0 4.0 5.0 6.0 7.0 8.0
(i)
0.0
−2.0 −1.0 0.0 1.0 2.0 3.0 4.0 5.0 6.0 7.0 8.0
(ii)
0.0
−2.0 −1.0 0.0 1.0 2.0 3.0 4.0 5.0 6.0 7.0 8.0
(iii)
Dimensionless Pressure (P)
0
−10
−20
−30
−40
Centreline pressure (Pc)
Wall pressure (Pw)
−2.0 −1.0 0.0 1.0 2.0 3.0 4.0 5.0 6.0 7.0 8.0
(iv)
0.0
−2.0 −1.0 0.0 1.0 2.0 3.0 4.0 5.0 6.0 7.0 8.0
(v)
Wall vorticity (ζ_w)
75
50
25
0
−2.0 −1.0 0.0 1.0 2.0 3.0 4.0 5.0 6.0 7.0 8.0
(vi)

Figure 4.

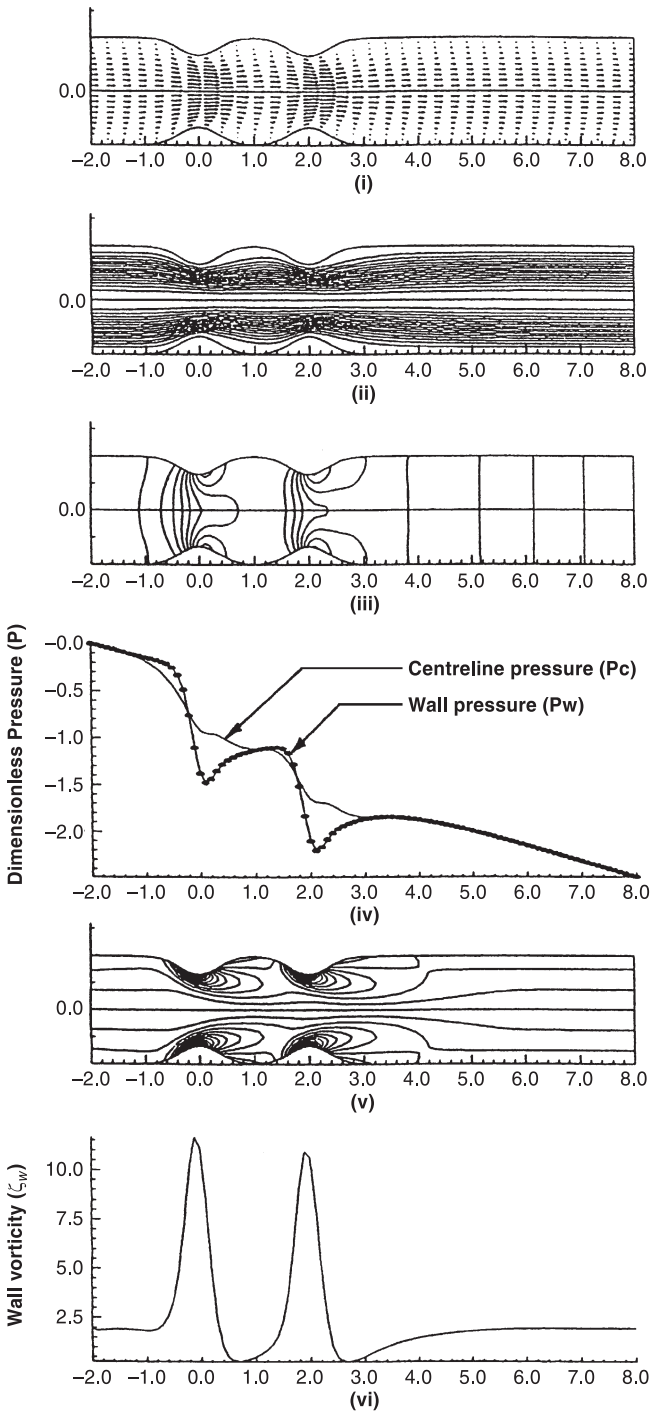

Figure 5.
(a) Re = 25; $c_1 = c_2 = 1/3$ (i) Velocity vectors; (ii) Streamlines; (iii) Pressure contours; (iv) Centreline (Pc) and Wall (Pw) pressures; (v) Vorticity contours; (vi) Wall vorticity (ζ_w) (b) Re = 25; $c_1 = c_2 = 1/2$ (i) Velocity vectors; (ii) Streamlines; (iii) Pressure contours; (iv) Centreline (Pc) and Wall (Pw) pressures; (v) Vorticity contours; (vi) Wall vorticity (ζ_w) (c) Re = 25; $c_1 = c_2 = 2/3$ (i) Velocity vectors; (ii) Streamlines; (iii) Pressure contours; (iv) Centreline (Pc) and Wall (Pw) pressures; (v) Vorticity contours; (vi) Wall vorticity (ζ_w)

(*Continued*)

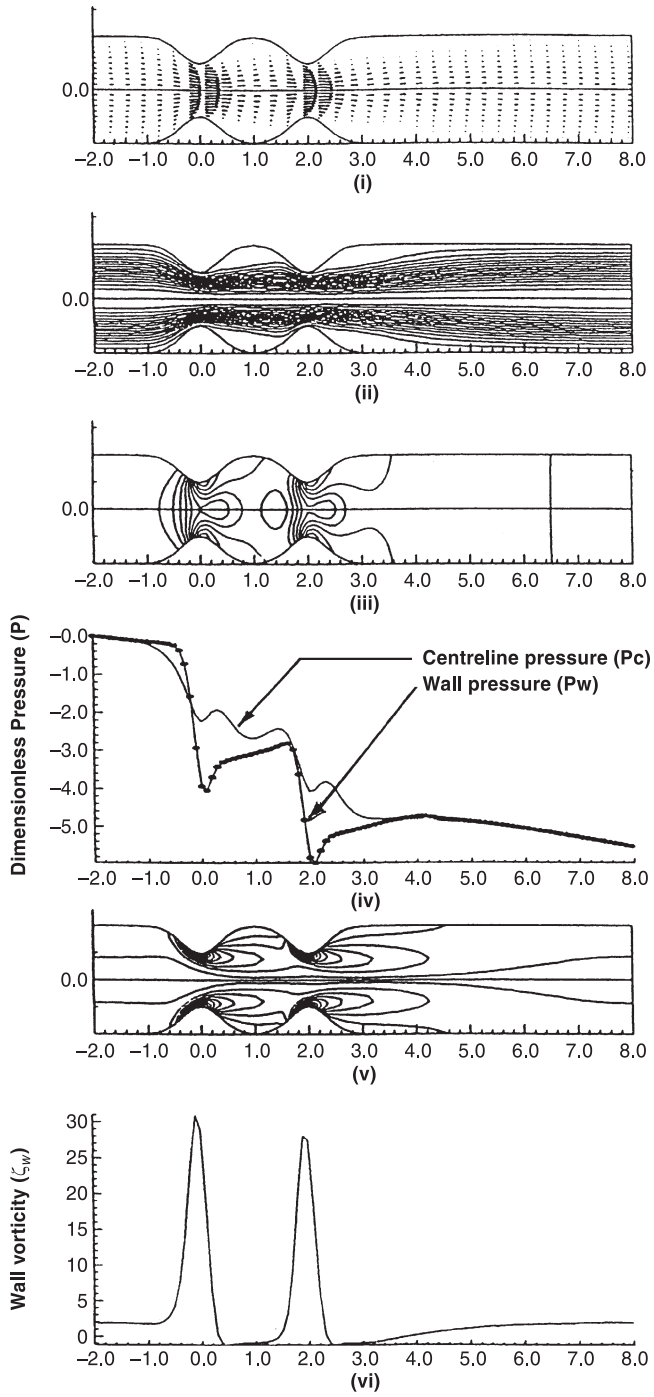

Figure 5.

(*Continued*)

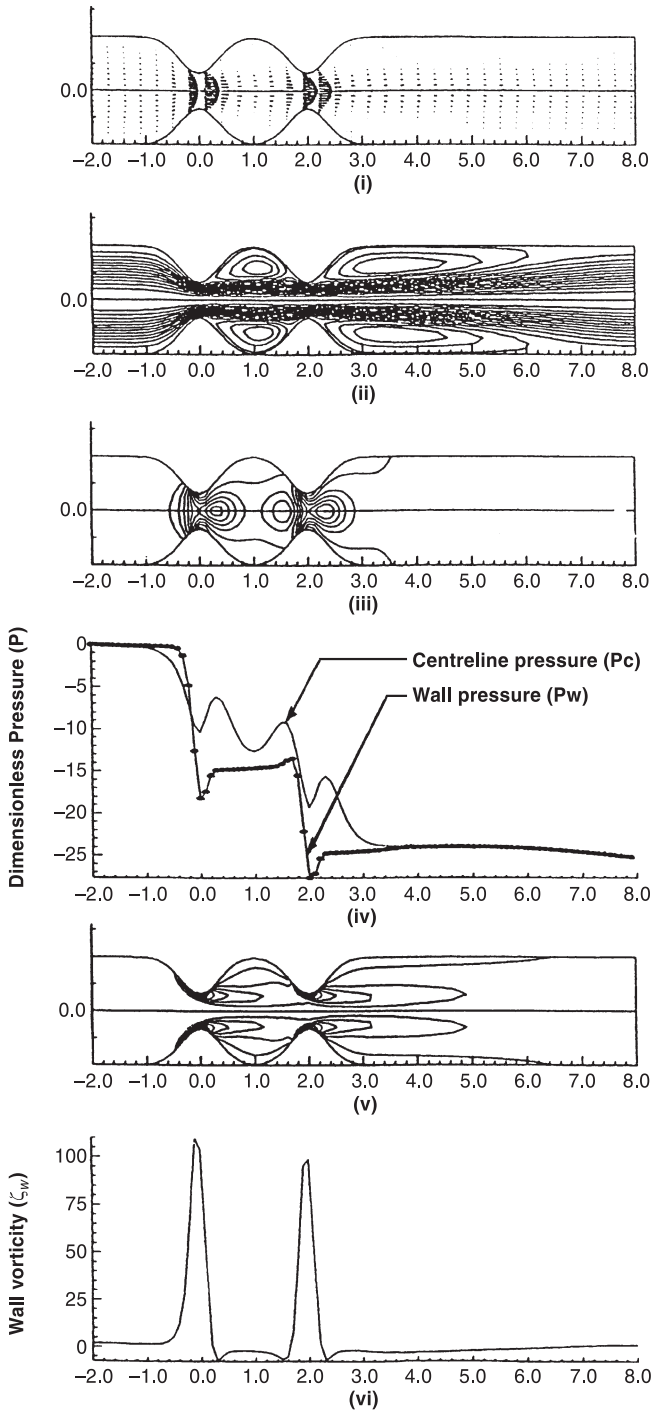
0.0
−2.0 −1.0 0.0 1.0 2.0 3.0 4.0 5.0 6.0 7.0 8.0
(i)
0.0
−2.0 −1.0 0.0 1.0 2.0 3.0 4.0 5.0 6.0 7.0 8.0
(ii)
0.0
−2.0 −1.0 0.0 1.0 2.0 3.0 4.0 5.0 6.0 7.0 8.0
(iii)
Dimensionless Pressure (P)
0
−5
−10
−15
−20
−25
Centreline pressure (Pc)
Wall pressure (Pw)
−2.0 −1.0 0.0 1.0 2.0 3.0 4.0 5.0 6.0 7.0 8.0
(iv)
0.0
−2.0 −1.0 0.0 1.0 2.0 3.0 4.0 5.0 6.0 7.0 8.0
(v)
Wall vorticity (ζ_w)
100
75
50
25
0
−2.0 −1.0 0.0 1.0 2.0 3.0 4.0 5.0 6.0 7.0 8.0
(vi)

Figure 5.

velocity increases in magnitude and the vectors point towards the axis of the tube. The formation of the recirculation region in the flow is indicated by the negative velocity vectors in a reversed flow. Thus, the profile distribution along an arterial vessel can be used to improve ways of detection of stenotic sites (Cavalcanti & Carota (1995)). The pressure characteristics are related to the velocity characteristics. The pressure distributions along the tube wall and along the centreline of the tube shown in Figures 4(iv) & (v) – 6(v) & (v). In general, there is a rapid fall in the pressure as the constriction is approached, with the pressure recovery after the second constriction taking place over a greater length. The wall vorticity values which are also related to the velocity distribution. The wall vorticity in turn is related to the tube wall shearing stress [$\tau_w = (\rho\upsilon V_\infty/a_0)\zeta_w$]. As shown in the corresponding Figures 4(vi)–6(vi), the magnitude of the wall vorticity values increase rapidly when the flow approaches the constriction and reaching a peak value near the maximum constricted area. At a higher Reynolds number, the peak wall vorticity value is found slightly upstream of the maximum constricted area. Downstream of this peak value, the wall vorticity decreases rapidly and will reverse to negative values when separation begins at the wall of the tube. It is observed that the peak wall vorticity value increases with increasing Reynolds number. The peak wall vorticity value tends to shift upstream as the Reynolds number is increased. The negative wall vorticity values also give an indication of the extend of the recirculation region in the constricted flow. For Reynolds number greater than a critical value for a given constriction, negative wall vorticity values are found at the tube surface due the existence of the recirculation eddy downstream of the constriction. The negative magnitudes of the wall vorticity values in the recirculation region increases when the Reynolds number is increased. For the present study with Reynolds number approaching 400, there is a large region of recirculatory flow in the constricted tube as evidence by the extent of negative wall vorticity distribution along the tube wall (Figure 7(a)–(d)). With $S = 1$, the recirculation eddy formed downstream of the first constriction has a deminishing effects on the generation of vorticities by the main stream near the second constriction area. The main stream approaching the second constriction wall is straightened by the recirculation region formed between the valley. Hence the maximum wall vorticity generated by the first constriction is always greater than the maximum wall vorticity generated by the second constriction. For constrictions of 1/3, 1/2 and 2/3, the maximum wall vorticity values obtained when the flow passes through the second constriction are always lower than those obtained in the corresponding cases for a constriction spacing $S = \infty$ or flow with single constriction.

From the above, it can be seen that for Re $<$ critical Re, the 1st constriction has no effect on the 2nd constriction and they behaves as independent entities. As Re rises above the critical Re and beyond, flow separation and flow interference between the two constrictions starts to occur. Eddies and

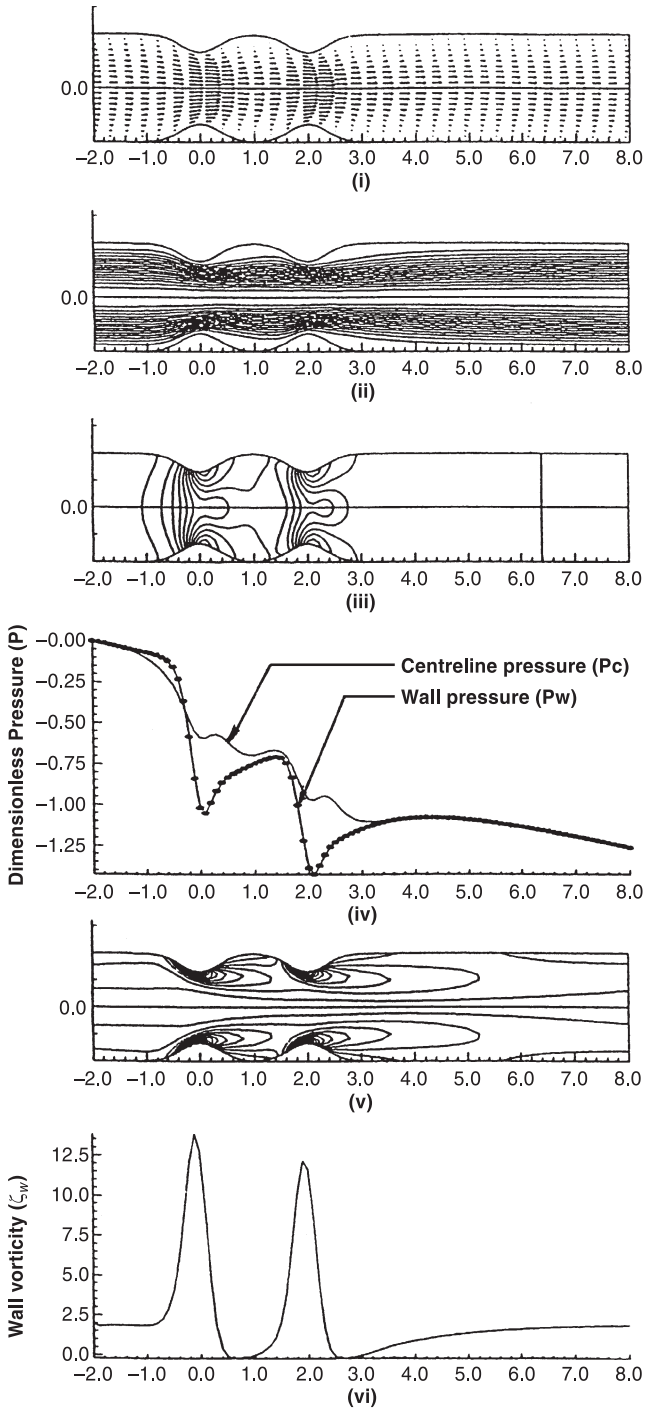

Figure 6.
(a) Re = 50; $c_1 = c_2 = 1/3$ (i) Velocity vectors; (ii) Streamlines; (iii) Pressure contours; (iv) Centreline (Pc) and Wall (Pw) pressures; (v) Vorticity contours; (vi) Wall vorticity (ζ_w) (b) Re = 50; $c_1 = c_2 = 1/2$ (i) Velocity vectors; (ii) Streamlines; (iii) Pressure contours; (iv) Centreline (Pc) and Wall (Pw) pressures; (v) Vorticity contours; (vi) Wall vorticity (ζ_w) (c) Re = 50; $c_1 = c_2 = 2/3$ (i) Velocity vectors; (ii) Streamlines; (iii) Pressure contours; (iv) Centreline (Pc) and Wall (Pw) pressures; (v) Vorticity contours; (vi) Wall vorticity (ζ_w)

(*Continued*)

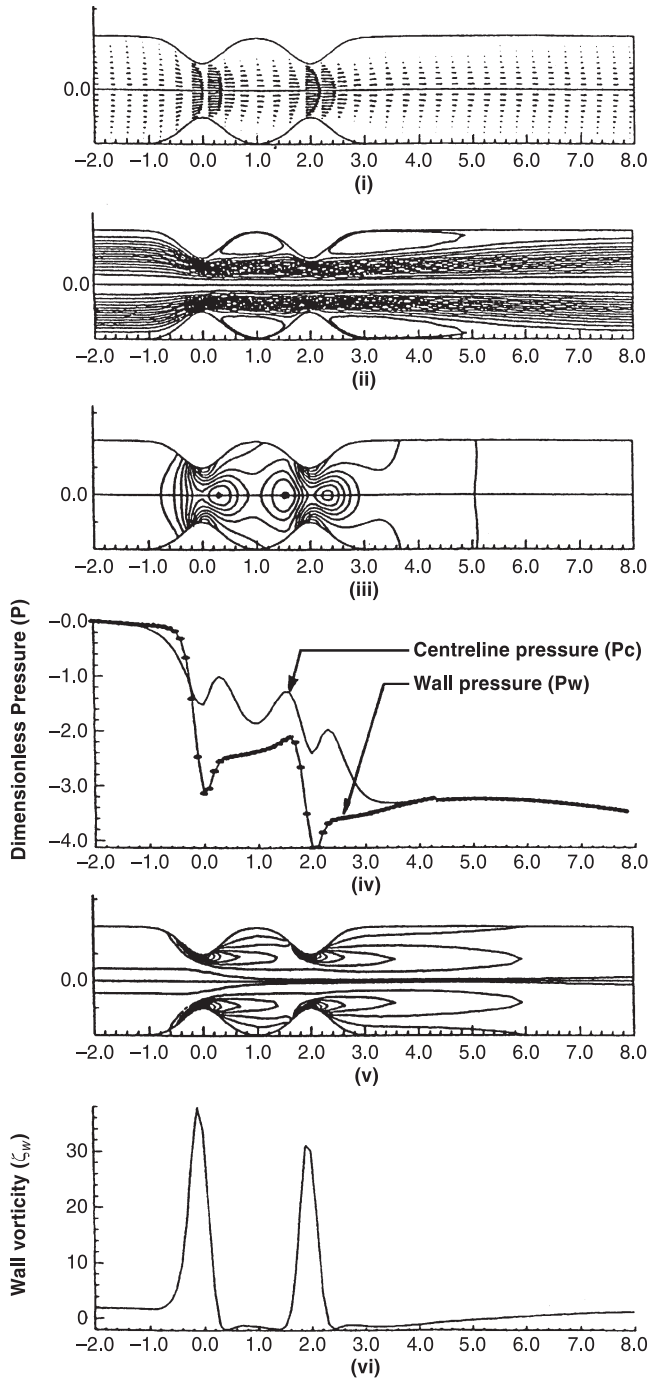

Figure 6.

(*Continued*)

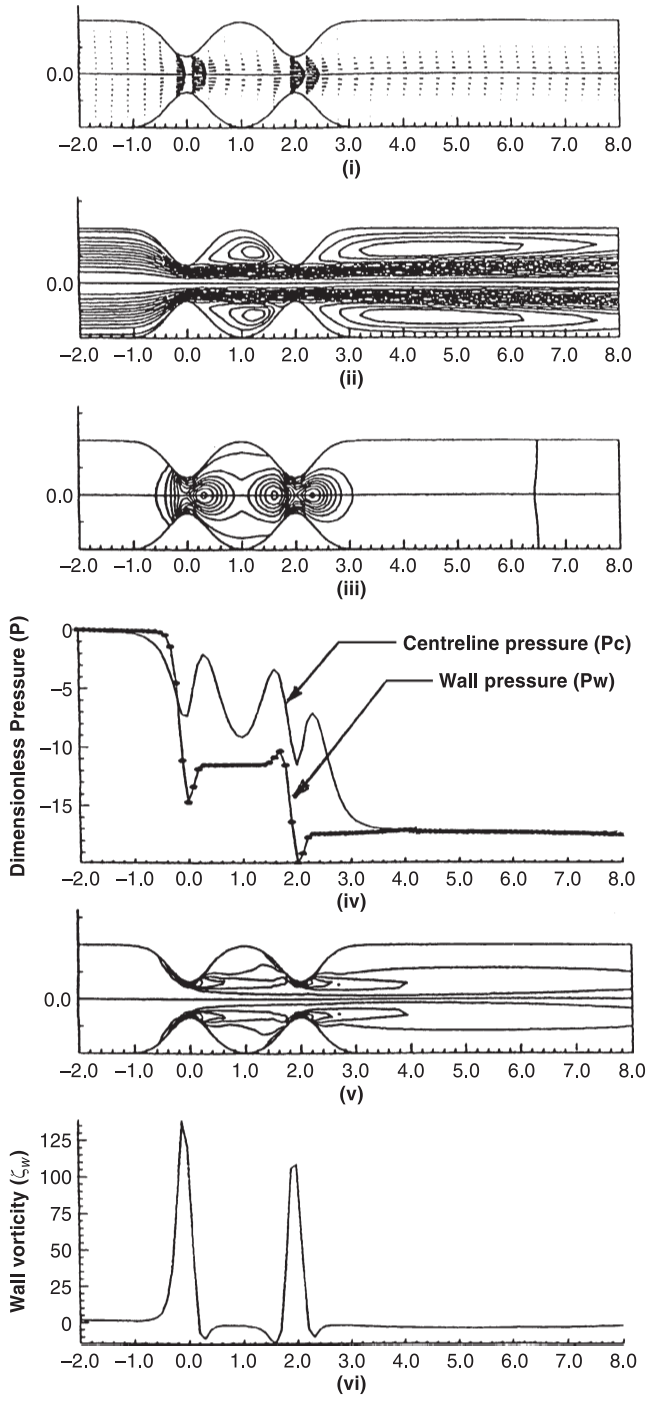
0.0
−2.0 −1.0 0.0 1.0 2.0 3.0 4.0 5.0 6.0 7.0 8.0
(i)
0.0
−2.0 −1.0 0.0 1.0 2.0 3.0 4.0 5.0 6.0 7.0 8.0
(ii)
0.0
−2.0 −1.0 0.0 1.0 2.0 3.0 4.0 5.0 6.0 7.0 8.0
(iii)
Dimensionless Pressure (P)
0
−5
−10
−15
Centreline pressure (Pc)
Wall pressure (Pw)
−2.0 −1.0 0.0 1.0 2.0 3.0 4.0 5.0 6.0 7.0 8.0
(iv)
0.0
−2.0 −1.0 0.0 1.0 2.0 3.0 4.0 5.0 6.0 7.0 8.0
(v)
Wall vorticity (ζ_w)
125
100
75
50
25
0
−2.0 −1.0 0.0 1.0 2.0 3.0 4.0 5.0 6.0 7.0 8.0
(vi)

Figure 6.

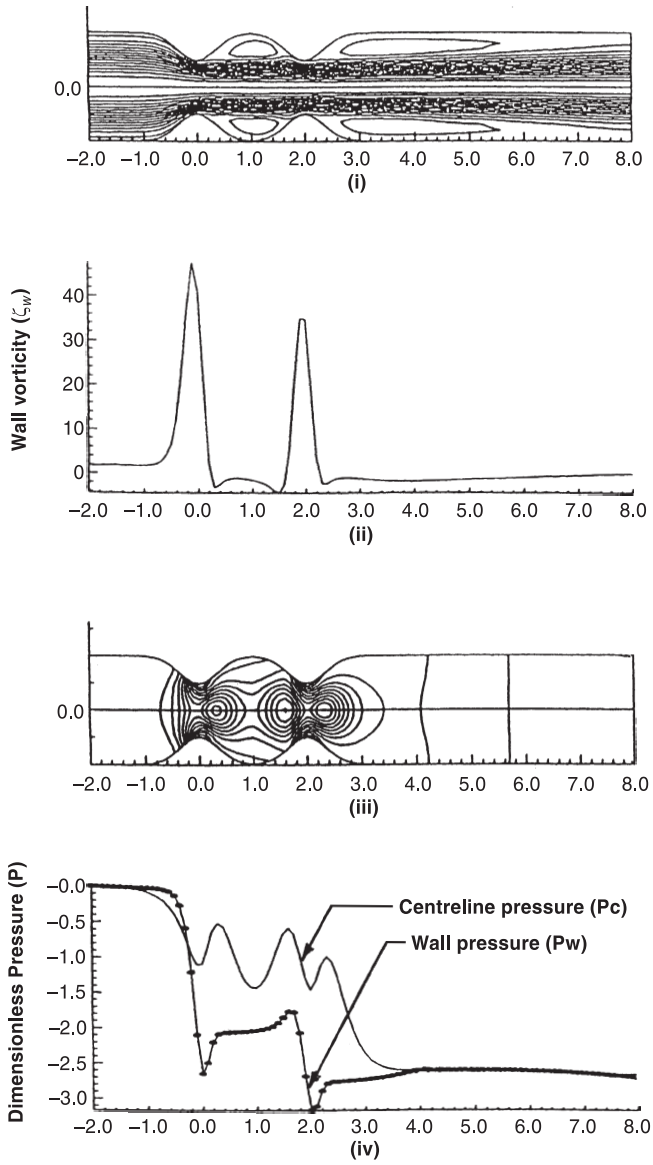

Figure 7.
(a) Re = 100; Figure 7(a)–(d) $c_1 = c_2 = 1/2$ (i) Streamlines; (ii) Wall vorticity (ζ_w); (iii) Pressure contours; (iv) Centreline (Pc) and Wall (Pw) pressures (b) Re = 200; $c_1 = c_2 = 1/2$ (i) Streamlines; (ii) Wall vorticity (ζ_w) (iii) Pressure contours; (iv) Centreline (Pc) and Wall (Pw) pressures (c) Re = 300; $c_1 = c_2 = 1/2$ (i) Streamlines; (ii) Wall vorticity (ζ_w) (iii) Pressure contours; (iv) Centreline (Pc) and Wall (Pw) pressures (d) Re = 400; $c_1 = c_2 = 1/2$ (i) Streamlines; (ii) Wall vorticity (ζ_w); (iii) Pressure contours; (iv) Centreline (Pc) and Wall (Pw) pressures

(*Continued*)

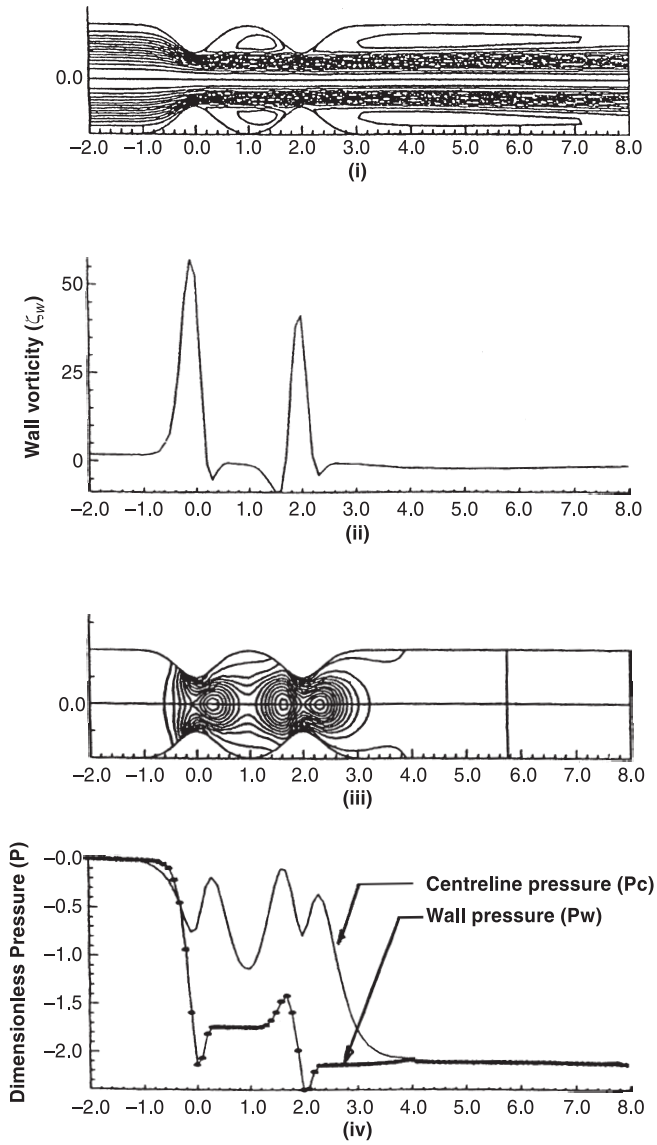

Figure 7.

(*Continued*)

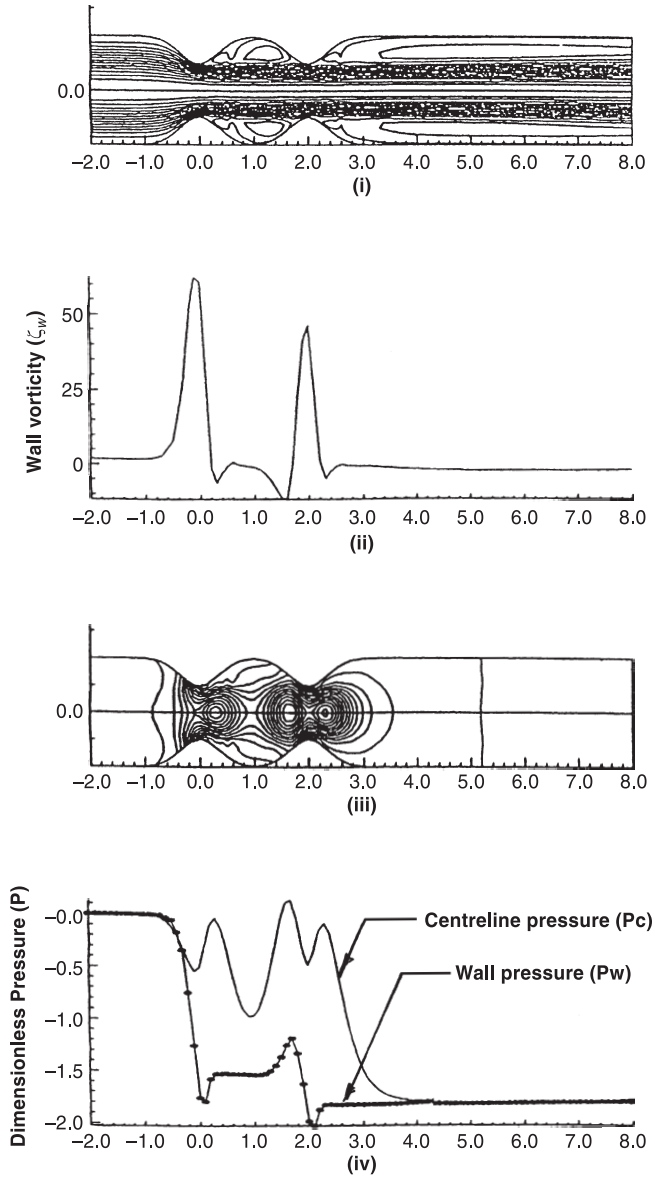

Figure 7.

(*Continued*)

recirculation regions develop after the narrowest point of the constriction and they separated from the main flow, with reattachment occurring further downstream. The reattachment points tend to extend downstream as Re increases. Recirculation regions are generally slow moving flow separated from the main stream, which can be seen from the streamline and velocity vector plots. At higher Re, due to the presence of the 2nd constriction, the recirculation regions generated by the first constriction will be trapped within the entire valley while that generated by the 2nd constriction will extend downstream. The velocity vector plots showed negative vectors in such recirculation regions. The convergence of the velocity vector heads as the flow approach the constriction and subsequent fanning out of the vectors showed adverse pressure gradient conducive to the formation of recirculation regions. Since the recirculation regions are trapped between the valley created by the 2 constrictions as Re increases, they straightened the flow approaching the 2nd constriction, resulting in rounder velocity profiles and lower wall vorticity at the downstream constriction.

The wall shear stress, τ_w, is an important parameter in atherosclerosis and is directly related to the wall vorticity (ζ_w). Figures 4(vi)–6(vi) show the nature of the wall shear stress variation in the axial direction for constriction ratios of 1/3, 1/2 and 2/3. The peak value of τ_w increases with an increase in Reynolds number. The wall shear stress value increases rapidly as the flow approaches the constriction and reaches a peak value near the maximum constricted area. Downstream of the constriction τ_w decreases rapidly and reverses sign which indicates a separation in the flow near the wall of the tube. An increase in Reynolds number causes the magnitude of the negative τ_w value to increase downstream of the constriction. This is due to an increase in the size of the recirculation region. The wall vorticity is similar to τ_w as they are directly related in Newtonian flows. The maximum value of the wall shear generated by the first constriction is always greater than the maximum value of the wall shear generated by the second constriction. This is because the recirculation eddy formed downstream of the first constriction has a diminishing effect on the vortices generated by the main stream near the second constriction area.

Figure 8 shows the pressure losses w.r.t. the constrictions and Reynolds number. For Re $<$ critical Re of a constriction value, the fall in pressure (or loss in energy) as the flow encounter the constrictions are the same, but as Re increases above critical Re, it can be seen that the fall in pressure is smaller in the 2nd constriction. A greater drop in pressure is seen as more energy being used up to overcome a greater resistance presented by the constriction. Mentioned in the earlier discussion, the flow is being straightened after passing through the 1st constriction by the recirculation region trapped within the valley between the 2 constrictions and this enables the flow to pass more "smoothly" with less resistance through the 2nd constriction, hence resulting in lower pressure loss at the 2nd constriction. Figures 4–7 also shows that the wall and centreline pressure for flow corresponding to Re $<$ critical Re, both

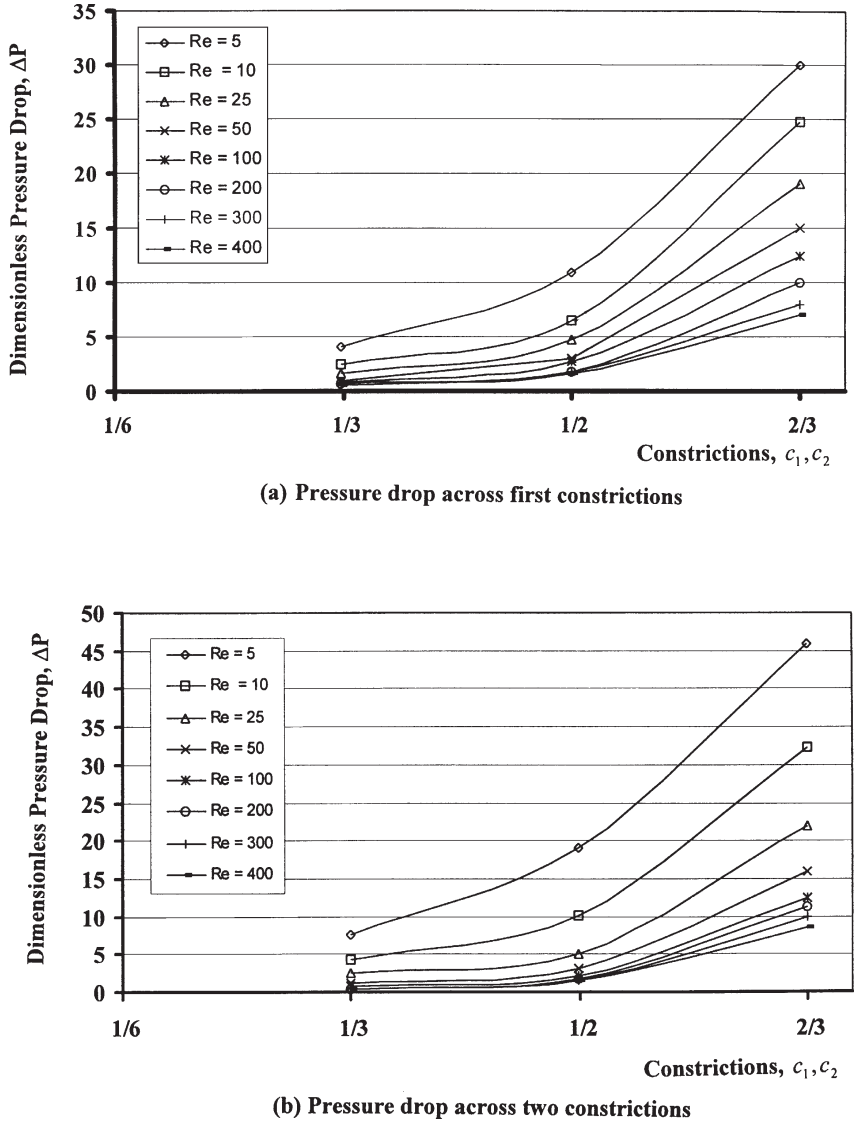

Figure 8.
Dimensionless pressure drop across constrictions

centreline and wall pressure are similar except at the constriction regions. The steeper gradient of the wall pressure plots over the constrictions as compared to the rest of the tube implies that pressure loss is greater at the wall. After a steep drop in wall pressure, there usually fellows a period of pressure recovery signalled by a rise in pressure. The graph shows that for Re $\gg$ critical Re, the pressure recovery phase after the 2nd constriction is stretched out over a much longer distance downstream compared to that of Re $<$ critical Re. The pressure

flow relationship is also one means of obtaining information about the severity of a coronary stenosis. For a given Reynolds number, the presence of a constriction increases the resistance that the flow experiences. Figure 8 generally showed that the pressure drop across two constrictions with spacing $S = 1.0$ is always less than twice the pressure drop over the first constriction. The above Investigations showed that the most important factors, which influence the pressure drop across multiple stenoses, are the cross-sectional area (diameter) reduction of each stenosis, the distance S between the stenosies and the Reynolds number. Investigations show that if the consecutive constrictions was closed enough, interference occurs with the normal expansion of the jet emerging from the proximal stenosis, changing the pressure drop at certain flow rates. The vortex behind the neighbouring stenosis appears to play an important role in the mutual interaction of both stenoses on the flow.

Figure 9 further shows details of the maximum wall vorticity plot for the three constriction settings at various Re. As can be seen from the figure, the increase in wall vorticity is more than double when the constriction ratio increased from 1/3 to 1/2 and is around 10 times as the constriction ratio rises to 2/3. This implies that the shear stress experienced at the wall may tripled and rises to 10 times for the constriction ratios increasing from 1/3 to 1/2 and from 1/3 to 2/3 respectively. There is an exponential rise in wall vorticity as the constriction ratio increases. Similarly, Figure 9 also shows that the maximum wall vorticity increases with increasing Reynolds number and constriction ratios. The peak wall vorticity values for the upstream constriction are the same as the corresponding cases for a single constriction. However, the peak wall vorticity generated by the first constriction is always greater than the peak wall vorticity generated by the second constriction. This difference indicates flow interference. The recirculation eddy formed downstream of the first constriction has a diminishing effect on the generation of vorticity by the main stream near the second constriction area. The main stream approaching the second constriction wall is straightened by the recirculation region formed between the valley.

Figure 10 shows the separation and reattachment points of the recirculation eddies formed downstream of each of the constrictions for different constriction ratios. It can be seen that when the Reynolds number is increased, the separation point on the surface of the constriction where the recirculation eddy begins to form, moves slightly upstream of the throat. The reattachment point where the recirculation eddy terminates on the surface of the constricted tube, spread downstream of the throat. When a steady recirculation region is established between the two constrictions, there is then little change to the separation and reattachment points for the flow between the valley region. However, the reattachment point of the downstream constriction spread further as the Reynolds number is increase and will eventually approaches that of a single constriction corresponding to $S = \infty$.

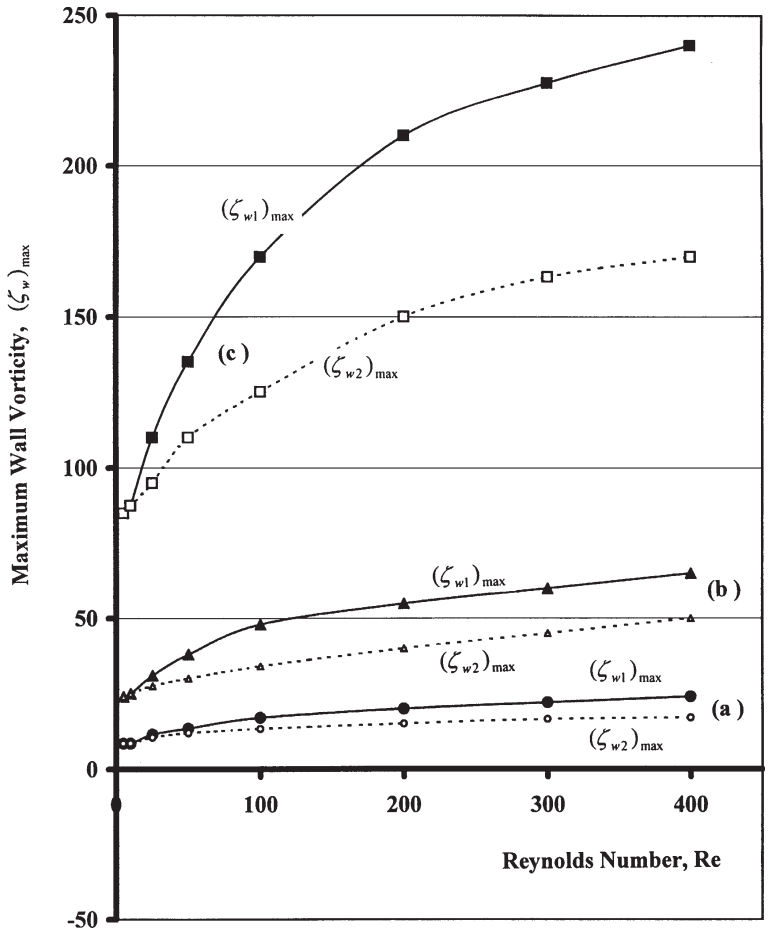

Figure 9.
Maximum wall vorticity at first and second constrictions $[(\zeta_{w1})_{max}; (\zeta_{w2})_{max}]$
(a) $c_1 = c_2 = 1/3$;
(b) $c_1 = c_2 = 1/2$;
(c) $c_1 = c_2 = 2/3$

Conclusion

Numerical solutions to the flow fields in the neighbourhood of double symmetrical bell-shaped constrictions in a circular cylindrical tube are obtained for a Reynolds number range of 5–400. The effect of the proximity of one constriction to another in term of a dimensionless spacing $S = 1$ is investigated. For the present study with a constriction of 1/3, 1/2 and 2/3, it is found that the formation of recirculation eddy occurs at downstream of the constriction when the Reynolds number is above a critical Reynolds number depending on the constriction magnitudes. For $c = 1/3$, 1/2 and 2/3, this critical Re is approximately at 5, 10 and 25, respectively. As the Reynolds number is increased above this critical Re, the point of separation of the eddy moves upstream of the constriction; and the point of reattachment of the recirculating flow moves downstream. At high

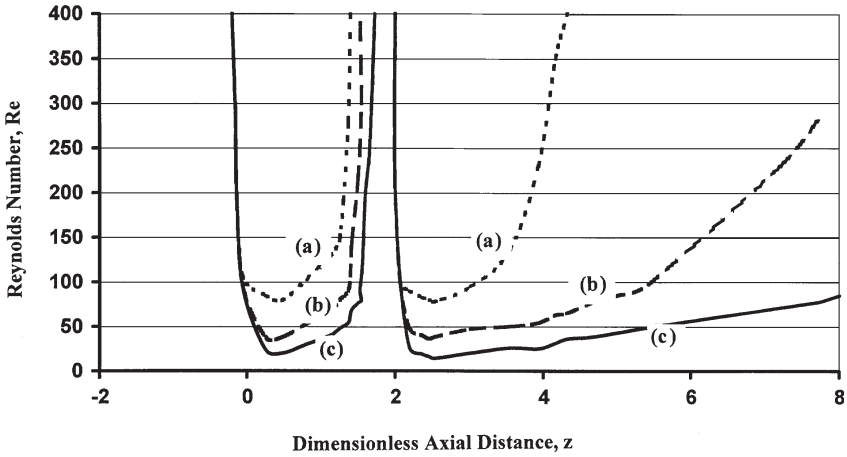

Figure 10.
Flow separation and re-attachment at first and second constrictions
(a) $c_1 = c_2 = 1/3$;
(b) $c_1 = c_2 = 1/2$;
(c) $c_1 = c_2 = 2/3$

Reynolds numbers, a recirculation zone exists which fills the valley region between the two constrictions. A separation streamline divides the flow in between the two constrictions into two parts: the recirculation region in the valley of the two constrictions, and a relatively straight and parallel flow near the centre of the tube. The net effects of these flow pattern is to reduce the maximum wall vorticity values downstream of the second constriction. The effects on the upstream vorticity and streamline pattern of the first constriction is small. The centreline pressure and wall pressure distribution and pressure losses through the flow were also very much affected by the flow pattern generated by the existence of the second constriction. As the flow approaches the narrowest section of the tube, it is accelerated and the maximum centreline velocity occurs slightly downstream of the constriction. The centreline velocity does not necessarily recover fully after passing through the first constriction before reaching the second constriction. Hence, the maximum centreline velocity not only shifts downstream as the Reynolds number increases, the maximum value at the second constriction is also higher than the maximum value at the first constriction. On the contrary, the local maximum wall vorticity value always occurs slightly upstream of each of the constrictions. The maximum wall vorticity at the second constriction is always less than the maximum wall vorticity value at the first constriction due to the influence of the recirculation flow region formed between the two constrictions. For the above flow, the major part of the pressure drop across the constrictions occurs just in front of each of the constrictions. The minimum pressures occurs just downstream of each of the constrictions.

References

Cavalcanti, S. and Carota, L. (1995), "Velocity profile distribution along an arterial vessel: way to improve detection of stenotic sites", *Med. & Biol. Engr. & Comput.*, 33, pp. 247-51.

Cieslicki, K. and Lasowska, A. (1999), "Experimental investigations of steady flow in a tube with circumferential wall cavity", *J. Fluids Engineering*, 121, pp. 405-9.

Cheng, T., Deville, M., Dheur, L. and Vandershcuren, L. (1992), "Finite element simulation of flow through arterial stenosis", *J. Biomech.*, 25, pp. 1141-52.

Deplano, V. and Siouffi, M. (1999), "Experimental and numerical study of flows through stenosis", *J. Biomechanics*, 32, pp. 1081-90.

Dreumel, S.C. and Kuiken, G.D.C. (1989), "Steady flow through a double converging-diverging tube model for mild coronary stenoses", *J. Biomech. Engr.*, 111, pp. 212-21.

Damodaran, V., Rankin, G.W. and Zhang, C. (1996), "Numerical study of steady laminar flow through tubes with multiple constrictions using curvilinear coordinates", *Int. J. Num. Mtd. Fluids*, 23, pp. 1021-41.

Dash, R.K., Jayaraman, G. and Metha, K.N. (1999), "Flow in a catheterized curved artery with stenosis", *J. Biomechanics*, 32, pp. 49-61.

Deshpande, M.D., Giddens, D.P. and Mabon, R.F. (1976), "Steady laminar flow through modelled vascular stenoses", *J. Biomech.*, 9, pp. 165-74.

Forrester, J.H. and Young, D.F. (1970), "Flow through a converging-diverging tube and its implications in occlusive vascular disease", *J. Biomech.*, 3, pp. 297-316.

Hron, J., Malek, J. and Turek, S. (2000), "A numerical investigation of flows of shear thinning fluids with applications to blood rheology", *Int. J. of Numerical Methods in Fluids*, 32, pp. 863-79.

Huang, H., Modi, V.J. and Seymour, B.R. (1995), "Fluid mechanics of stenosed arteries", *Int. J. Engr. Sci.*, 33, pp. 815-28.

Johnston, P.R. and Kilpatrick, D. (1991), "Mathematical modelling of flow through an irregular arterial stenosis", *J. Biomech*, 24, pp. 1069-77.

Lee, T.S. (1994), "Mixed Recirculatory Flow in the Annuli of Stationary and Rotating Cylinders with Different Radius Ratios", *International Journal of Numerical Methods for Heat and Fluid Flow*, 4 No. 6, pp. 561-73.

Lee, T.S. (1998), "Numerical Study of Early Stages of An Impulsively Started Unsteady Laminar Flow Past Expanded Trapezoidal Cylinders", *International Journal of Numerical Methods in Heat and Fluid Flow*, 8 No. 8, pp. 934-55.

Lee, S.J. and Fung, Y.C. (1970), "Flow in locally constricted tubes at low Reynolds Numbers", *J. Appl. Mech.*, 37, pp. 9-16.

Najeme, A., Zagzoule, M. and Mauss, J. (1992), "Numerical analysis of flow in arterial stenoses", *Mech. Research Comm.*, 19, pp. 379-84.

Oberkamph, W.L. and Goh, S.C., "Numerical solution of incompressible viscous flow in irregular tubes", Proc. Int. Conf. Computational Methods in Non-Linear Mechanics, Uni. Of Texas, Austin, 1974, p.569-579.

Patankar, S.V., Liu, C.H. and Sparrow, E.M. (1977), "Fully developed flow and heat transfer in ducts having streamwise-periodic variations of cross-sectional area", *ASME J. Heat Transfer*, 99, pp. 180-6.

Prata, A.T. and Sparrow, E.M. (1984), "Heat Transfer and Fluid Flow Characteristics for Annulus of periodically varying cross section", *Numerical Heat Transfer*, 7, pp. 285-304.

Reese, J.M. and Thompson, D.S. (1998), "Shear stress in arterial stenoses: a momentum integral method", *J. Biomechanics*, 31, pp. 1051-7.

Rosenfeld, M. and Einav, S. (1995), "The effect of constriction size on the flow in a channel", *J. Fluid Engr.*, 117, pp. 571-6.

Sobey, I.J. (1980), "On flow through furrowed channels. Part I: Calculated flow pattern", *J. Fluid Mechanics*, 96, pp. 1-26.

Samarskii, A.A. and Andrew, V.B. (1963), "On high accuracy difference scheme for an elliptic equation with several space variables", *USSR Comp. Math. Physics*, 3, pp. 1373-83.

Sparrow, E.M. and Prata, A.T. (1983), "Numerical solutions of laminar flow and heat transfer in a periodically converging-diverging tube", *Numerical Heat Transfer*, 6, pp. 441-61.

Selvarajan, S., Tulaparkara, E.G. and Ram, V.V. (1998), "A numerical study of flow through wavy-walled channels", *Int. J. Numerical Methods in Fluids*, 26, pp. 519-31.

Siouffi, M., Deplano, V. and Pelissier, R. (1998), "Experimental analysis of flows through a stenosis", *J. Biomech.*, 31, pp. 11-19.

Stroud, J.S., Berger, S.A. and Saloner, D. (2000), "Influence of stenosis morphology on flow through severely stenotic vessels: implications for plaque rupture", *J. Biomechanics*, 33, pp. 433-55.

Tutty, O.R. (1992), "Flow in a constricted channel", *J. Biomech. Engr.*, 114, pp. 50-4.

Tsangaris, S. and Leiter, E. (1984), "On Laminar steady flow in sinusoidal channels", *Journal of Engineering Mathematics*, 18, pp. 89-103.

Wang, C.Y. (2001), "Flow in a channel with longitudinal tubes", *J.Fluids Engineering*, 123, pp. 157-60.

Young, D.F. and Tsai, F.Y. (1973), "Flow Characteristics in Models of Arterial Stenoses – I, Steady Flow", *J. Biomech.*, 6, pp. 395-410.

Zendehbudi, G.R. and Moayeri, M.S. (1999), "Comparison of physiological and simple flows through stenosed arties", *J. Biomechanics*, 32, pp. 959-65.